blood

2012 120: e9-e16
Prepublished online May 31, 2012;
doi:10.1182/blood-2012-03-414920

Reconstructing the human hematopoietic niche in immunodeficient mice: opportunities for studying primary multiple myeloma

Richard W. J. Groen, Willy A. Noort, Reinier A. Raymakers, Henk-Jan Prins, Linda Aalders, Frans M. Hofhuis, Petra Moerer, Jeroen F. van Velzen, Andries C. Bloem, Berris van Kessel, Henk Rozemuller, Ellen van Binsbergen, Arjan Buijs, Huipin Yuan, Joost D. de Bruijn, Michel de Weers, Paul W. H. I. Parren, Jan Jacob Schuringa, Henk M. Lokhorst, Tuna Mutis and Anton C. M. Martens

Blood (print ISSN 0006-4971, online ISSN 1528-0020), is published weekly by the American Society of Hematology, 2021 L St, NW, Suite 900, Washington DC 20036.

e-*Blood*

Reconstructing the human hematopoietic niche in immunodeficient mice: opportunities for studying primary multiple myeloma

Richard W. J. Groen,[1,2] Willy A. Noort,[1] Reinier A. Raymakers,[3] Henk-Jan Prins,[2] Linda Aalders,[1,2] Frans M. Hofhuis,[2] Petra Moerer,[2] Jeroen F. van Velzen,[2] Andries C. Bloem,[2] Berris van Kessel,[4] Henk Rozemuller,[2] Ellen van Binsbergen,[5] Arjan Buijs,[5] Huipin Yuan,[6] Joost D. de Bruijn,[6,7] Michel de Weers,[8] Paul W. H. I. Parren,[8] Jan Jacob Schuringa,[9] Henk M. Lokhorst,[3] Tuna Mutis,[4] and Anton C. M. Martens[1,2]

Departments of [1]Cell Biology, [2]Immunology, [3]Hematology, [4]Clinical Chemistry and Hematology, and [5]Medical Genetics, University Medical Center Utrecht, Utrecht, The Netherlands; [6]Xpand Biotechnology BV, Bilthoven, The Netherlands; [7]The School of Engineering and Materials Science, Queen Mary University of London, London, United Kingdom; [8]Genmab, Utrecht, The Netherlands; and [9]Department of Hematology, University of Groningen and University Medical Center Groningen, Groningen, The Netherlands

Interactions within the hematopoietic niche in the BM microenvironment are essential for maintenance of the stem cell pool. In addition, this niche is thought to serve as a sanctuary site for malignant progenitors during chemotherapy. Therapy resistance induced by interactions with the BM microenvironment is a major drawback in the treatment of hematologic malignancies and bone-metastasizing solid tumors. To date, studying these interactions was hampered by the lack of adequate in vivo models that simulate the human situation. In the present study, we describe a unique human-mouse hybrid model that allows engraftment and outgrowth of normal and malignant hematopoietic progenitors by implementing a technology for generating a human bone environment. Using luciferase gene marking of patient-derived multiple myeloma cells and bioluminescent imaging, we were able to follow pMM cells outgrowth and to visualize the effect of treatment. Therapeutic interventions in this model resulted in equivalent drug responses as observed in the corresponding patients. This novel human-mouse hybrid model creates unprecedented opportunities to investigate species-specific microenvironmental influences on normal and malignant hematopoietic development, and to develop and personalize cancer treatment strategies. (*Blood*. 2012;120(3): e9-e16)

Introduction

In the BM, specialized microenvironments such as hematopoietic niches regulate hematopoiesis. Within these niches, hematopoietic stem cells (HSCs) are present in a complex network consisting of mesenchymal stromal cells (MSCs), osteoblasts, osteoclasts, endothelial cells, and adipocytes embedded in an extracellular matrix. The bidirectional interactions with the hematopoietic niche are essential for HSC maintenance and function.[1-4]

The BM niche is also thought to serve as a sanctuary site for leukemic stem cells (LSCs), which, in addition to their immortalizing genetic events, highly depend on interaction with the microenvironment to survive and proliferate.[5,6] Although the majority of leukemias initially respond to therapeutic intervention, relapse rates are high.[7-9] There is increasing evidence that the tumor niche plays a crucial role in the survival and drug resistance of LSCs. Interactions with the niche provide signals protecting the LSCs from apoptosis and eventually leading to the selection and outgrowth of a resistant cell.[10-13] Therefore, it is apparent that the hematopoietic niche plays an important role in hematopoietic development and in chemotherapy resistance of BM-localized leukemic and solid tumors.

Although our understanding of how the BM niche regulates HSC self-renewal and confers therapy resistance has advanced greatly over the past years, most of this knowledge is based on genetic loss-of–function or gain-of-function murine models.[1,2,10,11,14] However, these murine models do not simulate human physiology and much of the constituents of the human hematopoietic niche remain largely unclear.[14-16] This emphasizes the need for more suitable models that recapitulate the human BM microenvironment and, very importantly, facilitate the engraftment and outgrowth of normal HSCs and patient-derived tumor cells within these protected sites.

In the present study, we describe a unique humanized model that implements a novel scaffold-based technology for generating a human bone environment in $RAG_2^{-/-}\gamma c^{-/-}$ mice.[17] Inoculation of these mice with $CD34^+$ hematopoietic progenitor cells isolated from umbilical cord blood resulted in homing to the human bone environment and differentiation into multiple blood cell lineages. The optimal supportive nature of these humanized niches was illustrated by the ability to maintain the growth of patient-derived multiple myeloma (pMM) cells. Using luciferase gene marking of MM cells and bioluminescent imaging, we could precisely visualize pMM outgrowth and the effect of treatment. We conclude that this novel human-mouse hybrid model provides the ideal conditions with which to investigate essential interactions within the human BM microenvironment in relation to the development of normal and malignant hematopoiesis, which may affect the outcome of cancer therapy.

Submitted March 1, 2012; accepted May 20, 2012. Prepublished online as *Blood* First Edition paper, May 31, 2012; DOI 10.1182/blood-2012-03-414920.

This article contains a data supplement.

The publication costs of this article were defrayed in part by page charge payment. Therefore, and solely to indicate this fact, this article is hereby marked "advertisement" in accordance with 18 USC section 1734.

Methods

Patients, animals, and ethics

All MM patient materials and normal BM aspirates were collected after written informed consent was approved by the institutional medical ethical committee. Mononuclear cells of MM patients were separated by Ficoll-Hypaque density-gradient centrifugation and stored at −196°C. For patient characteristics, please see supplemental Table 1 (see the Supplemental Materials link at the top of the article). All animal experiments were conducted after acquiring permission from the local ethical committee for animal experimentation and were in compliance with the Dutch Animal Experimentation Act.

Generation of a humanized bone environment in mice

Ossicles containing human bone were created as described previously.[17] In brief, 4 hybrid scaffolds consisting of three 2- to 3-mm biphasic calcium phosphate (BCP) particles loaded with human MSCs were implanted subcutaneously into RAG2$^{-/-}\gamma_c^{-/-}$ mice. In addition, 2 controls were implanted: 1 of 2 control scaffolds was loaded with MSCs but exposed to 30 Gy of x-rays just before implantation and the other was not loaded with cells.

Injection of the mice with MM cells

Eight weeks after transplantation, anesthetized mice (IsoFlo; Abbott) were inoculated with umbilical cord blood–derived CD34$^+$ cells or with pMM cells with or without prior viral gene marking with a luciferase containing construct. The injection was either intracardial (5×10^5 CD34$^+$ cells or 5×10^6 MM cells) to study active homing of the cells or was directly into the ossicles (1×10^5 CD34$^+$ cells or 1-2 $\times 10^6$ MM cells) to study the engraftment potential.

Gene marking of pMM cells and bioluminescent imaging

pMM cells were thawed and incubated for 6 hours in IMDM (Invitrogen) supplemented with 10% fetal clone I serum (Hyclone Laboratories), 20 μg/mL transferrin (Sigma-Aldrich), 50μM β-mercaptoethanol, 100 units/mL penicillin, and 100 μg/mL streptomycin (both Invitrogen). Subsequently, cells were incubated overnight with viral particles of the lentiviral construct pRRL-cPPT-CMV-Luc2-IRES-GFP-PRE-SIN,[18] 6 ng/mL polybrene (Sigma-Aldrich), and 20 ng/mL IL-6 (R&D Systems). The next day, cells were washed 4 times and injected into RAG2$^{-/-}\gamma_c^{-/-}$ mice. Transduction efficiency was determined using the FACSCanto II flow cytometer (BD Biosciences) 48 hours after transduction. Bioluminescent imaging was performed as described previously[19] except that beetle luciferin (Promega) was used. Mice were treated with 1 mg/kg dexamethasone or 2.5 mg/kg melphalan daily for 5 days or with 0.5 mg/kg bortezomib twice weekly for 4 weeks as described previously[20]; with 1.5 mg/kg doxorubicin on days 1, 3, and 5; or once with daratumumab 8 mg/kg (Genmab).

Immunohistologic analysis

Formalin-fixed, EDTA-decalcified paraffin-embedded tissue sections were either stained with H&E (Klinipath) or used for immunohistochemical analysis. Endogenous peroxidase activity was blocked with 0.3% H_2O_2 in methanol. For antigen retrieval, sections were boiled for 10 minutes in a citrate buffer, pH 6, and then blocked with serum-free protein block (DAKO). Next, the slides were incubated overnight at 4°C with anti-CD45 (2B11 + PD7/26; DAKO), anti-CD3 (A0452; DAKO), anti-CD15 (MMA; BD Biosciences), anti-CD20 (L26; DAKO), anti-CD34 (QBEnd10; Beckman Coulter), anti-CD38 (38C03; Neomarkers), anti-CD138 (IQP-153; IQ Products), or antiluciferase (CR2029 RAP; Cortex Biochem). Binding of the Ab was visualized using the PowerVision Plus detection system (Immunovision Technologies) and 3,3-diaminobenzidine (Sigma-Aldrich). The sections were counterstained with hematoxylin, washed, and subsequently dehydrated through graded alcohol, cleared in xylene, and coverslipped. Tartrate-resistant acidic phosphatase staining was performed by incubating slides for 20 minutes in 0.2M acetate at room temperature. Next, the sections were incubated with 0.5 mg/mL naphthol AS-MX phosphate (Sigma-Aldrich) and 1.1 mg/mL of Fast Red TR salt (Sigma-Aldrich) in 0.2M acetate for 1 hour at 37°C. Finally, the sections were rinsed in distilled water, stained with hematoxylin for 2 minutes, washed under running tap water, air dried, and coverslipped. Images were captured using an Axiostar light microscope (Zeiss) with AxioVision Version 4.6 image analysis software (Zeiss).

Flow cytometry

Cells retrieved from humanized mice and inoculated with pMM cells were analyzed using an RPE-conjugated Ab directed against human CD138 (B-A38; Beckman Coulter). Analysis was carried out on a FACSCanto II flow cytometer with FACSDiva Version 6.1.3 software (BD Biosciences).

FISH analysis

FISH analyses were performed on cultured MM BM cells and pMM cells derived from mouse ossicles according to standard procedures using the probes LSI IGH/FGFR3 DCDF, LSI IGH/MAF DCDF, LSI IGH/CCND1 DCDF, LSI D5S23/D5S721, CEP9, CEP15, LSI13, and LSIp53 (Abbott-Vysis).

Results

We described recently an optimized procedure for the in vivo generation of human bone from MSCs in BCP scaffolds.[17] Subcutaneous placement of BCP scaffolds seeded with MSCs in immunodeficient mice resulted in the outgrowth of human osteoblasts and the deposition of human bone throughout the scaffolds within 8 weeks (Figure 1A left panel). Close ex vivo examination of the so-called ossicles revealed that the open spaces were vascularized and contained various types of murine hematopoietic cells (Figure 1A right panel). Culturing of cells isolated from the ossicles in an in vitro colony assay showed the outgrowth of granulocyte-macrophage colonies (CFU-GM), indicating the presence of murine myeloid progenitor cells (data not shown). To investigate whether the ossicles could also support human hematopoiesis, mice carrying humanized scaffolds were inoculated with CD34$^+$ cells isolated from umbilical cord blood either by injection directly into the ossicles or by intracardiac injection. This not only resulted in engraftment of CD34$^+$ hematopoietic progenitor cells themselves, but also in the production of human hematopoietic cells of distinct lineages (Figure 1B).

The supportive nature of these humanized niches was further investigated with pMM cells, a hematopoietic malignancy that is highly dependent on the BM microenvironment for survival and growth.[21-23] RAG2$^{-/-}\gamma_c^{-/-}$ mice were implanted with 4 MSC-loaded BCP scaffolds to create a humanized bone environment. There were 2 control scaffolds, one loaded with MSCs but exposed to 30 Gy of x-rays just before implantation and the other not loaded with cells. Humanized mice were inoculated with pMM cells from 7 patients (supplemental Table 1) either by injection directly into the ossicles or by intracardiac injection. For all 7 patients, both injection procedures resulted in tumor development within the humanized bone environment (Figure 2A-B). We also found circulating CD138$^+$ cells in the peripheral blood of the mice (Figure 2C). In contrast, none of the 7 pMM cells engrafted in the control "naked" scaffolds, and only 1 of them (patient 7) showed some engraftment in the murine BM. Furthermore, for 3 patients (patients 3, 4, and 7), the engraftment study was replicated in 3 or more separate experiments using different aliquots from the same

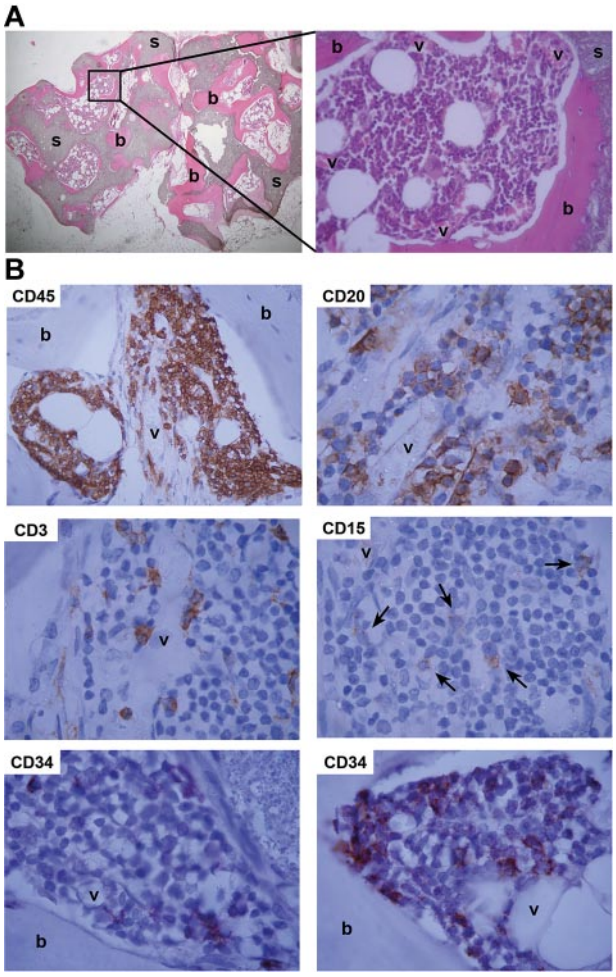

Figure 1. Artificial humanized bone microenvironment acts as a natural hematopoietic niche. (A) To generate a humanized bone environment, RAG2$^{-/-}\gamma_c^{-/-}$ mice were implanted with human MSC-loaded BCP scaffolds (s). Eight weeks after implantation, this led to the formation of human bone (b) in the vascularized (v) open spaces that was capable of supporting mouse hematopoiesis. Representative H&E-stained slides are shown. (B) CD34$^+$ UCB cells engraft and differentiate in humanized ossicles. RAG2$^{-/-}\gamma_c^{-/-}$ mice implanted with MSC-loaded BCP scaffolds and injected with CD34$^+$ cells at week 8 and analyzed at week 16 revealed ossicles with human CD45$^+$ cells (CD45). These included B cells (CD20), T cells (CD3), and myeloid cells (CD15). Undifferentiated CD34$^+$ cells (CD34) were detected adjacent to both bone (b) and vessels (v). Shown are representative images of immunohistochemical stainings for human CD markers.

initial pMM samples. In addition, pMM cells harvested from engrafted humanized mice from patients 4 and 7 resulted in pMM outgrowth in secondary recipient mice (data not shown). These data confirmed the consistency and reproducibility of pMM samples injected in our humanized mice.

To evaluate whether the initial genetic aberrations found in the original tumor were still present in the pMM cells growing in the humanized mice, we isolated the tumor cells of patient 4 from the scaffolds inoculated in 2 different mice and performed a comparative genetic analysis of these cells with the original malignant cells. In the original tumor, 84% of the cells displayed a t(4;14)(p16;q32) translocation (Figure 2D top panel); 62% of the cells lacked 1 copy of the tumor suppressors *TP53* and *RB1*. Analysis of the cells obtained from the 2 mice revealed the presence of all 3 aberrations in 100% of the cells (Figure 2D bottom panel). In addition, the pMM cells retrieved from both mice contained approximately 30% and 100% tetraploid cells, respectively, an aberration that was not detected in the original tumor. These data indicate that the initial aberrations were still present in the pMM cells that were engrafted and growing in the humanized mice. The progression of the tumor in mice most probably paralleled the clinical situation, because clinical progression (ie, tetraploidy) has been associated with the loss of *RB1* and *TP53*.[24,25] Analysis of a second patient (patient 7) also showed that the aberrations present in the original tumor were still present in the pMM cells obtained from patient 7 MM-bearing mice (supplemental Figure 1).

In addition to the observation that pMM cells could engraft and grow in the humanized bone environment, we noted that 1 of the major sequela of MM, the development of osteolytic lesions and/or diffuse osteopenia, also occurred in our model. Under physiologic conditions, structural remodeling of the bone is a continuous process in which osteoclasts mediate resorption of "old" bone tissue, which is balanced by new bone formation by osteoblasts. In MM, however, these 2 processes are uncoupled because of increased osteoclast activation and suppression of osteoblast function.[26-29] When we inoculated our humanized scaffolds with pMM cells, the normally smooth bone surface became irregular (Figure 3A), suggesting active resorption of the bone presumably by osteoclasts. It was also interesting that noninjected and patient acute myeloid leukemia–injected ossicles contained low numbers of osteoclasts that resided on the BCP surface, but not on the bone surface (Figure 3B left and middle panels), whereas ossicles injected with pMM cells contained high numbers of osteoclasts that lined the surface of the bone with MM cells in close proximity (Figure 3B right panel).

To gain insight in the engraftment pattern, growth dynamics, and response to therapy, we transduced pMM cells with a lentiviral luciferase construct[18] that enabled us to follow in vivo MM cell growth noninvasively by bioluminescent imaging (BLI).[30] As shown in Figure 4A, 17% of the primary CD138$^+$ MM cells were gene marked after lentiviral transduction without marking any of the CD138$^-$ cells present in the patient sample (data not shown). Without further selecting for the gene-marked population, this cell preparation was inoculated via intra-scaffold injection into mice carrying humanized ossicles or via subcutaneous injection into control mice without implants (Figure 4B). Monitoring the tumor growth with BLI revealed that pMM cells could only expand in mice with established ossicles containing human bone (Figure 4C). Furthermore, we observed that, within individual mice, noninjected humanized ossicles became colonized by pMM cells (Figure 4D), indicating active circulation, homing, and re-engraftment of the pMM cells into other human niches. Postmortem immunohistochemical analysis for luciferase showed that the MM tumors contained a mixture of positive and negative cells (Figure 4E), indicating that no selective outgrowth had occurred. The fact that no BLI signal could be detected in mouse bones confirmed the inability of mouse BM to support the engraftment of pMM cells. Consistent with our previous studies,[30] MM monitoring by BLI was superior to monitoring paraprotein levels in the serum of the mice. Using BLI, we could already detect MM growth from day 4 on compared with first detection starting at day 50 for paraprotein monitoring (data not shown).

Because BLI not only allows visualization but also quantification of pMM outgrowth, we tested the feasibility of using this novel humanized model to monitor therapeutic intervention. First, we applied total body irradiation with a dose of 6 Gy x-rays to a pMM-bearing humanized mouse. This resulted in a tumor load reduction of $>95\%$ (Figure 4F). Next, we investigated the suitability of the model to monitor the effect of chemotherapy. Mice that were inoculated with the luciferase-marked pMM cells of

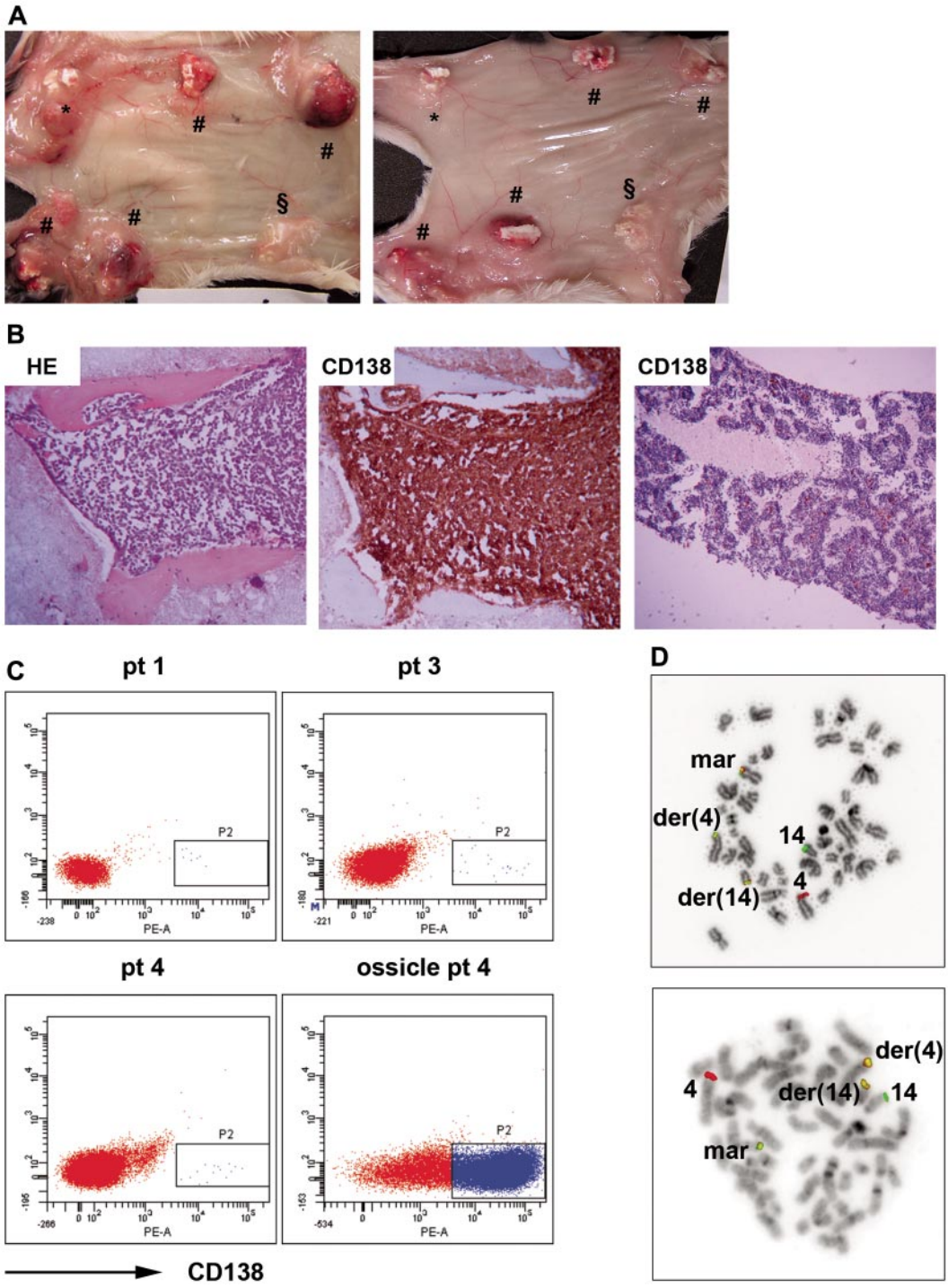

Figure 2. Humanized mice allow engraftment and growth of primary MM cells. (A) Mice were implanted with 4 MSC-loaded BCP scaffolds (#); one control was loaded with MSCs and exposed to 30 Gy of x-rays before implantation (*) and the other control was without MSCs (§). Mice were inoculated with mononuclear cells (MNCs) from patient 3 either directly into the ossicles (left panel) or by intracardiac injection (right panel). Representative images of ossicles inoculated via both injection procedures are shown. (B) Immunohistochemical sections of an ossicle from a humanized mouse inoculated with MNCs of patient 4 stained by HE (left panel) or anti–human CD138 (middle panel), and the femur of the corresponding mouse stained by anti–human CD138 (right panel). Representative pictures are shown. (C) Flow cytometric analysis of the blood and ossicles of humanized mice with anti–human CD138. Representative flow cytometry plots of the blood of mice inoculated with MNCs of patient 1, 3, and 4, and cells retrieved from an ossicle of a mouse inoculated with MNCs of patient 4 are shown. (D) FISH analysis of MNCs of patient 4 and cells retrieved from an ossicle of a mouse inoculated with MNCs of patient 4 for t(4;14)(p16;q32). Shown are 2 representative pictures hybridized with the LSI IGH/FGFR3 probes of metaphase cells of patient 4 (top panel) and corresponding mouse (bottom panel). der(4) indicates derivative chromosome 4; der(14), derivative chromosome 14; mar, marker chromosome; and 4 and 14, normal copies of chromosomes 4 and 14.

patient 3 (supplemental Table 1) were treated with the same chemotherapeutics that were used to treat the patient. This patient had become resistant to PAD (bortezomib, Adriamycin, dexamethasone) chemotherapy at the time the MM sample was collected. Thereafter, the patient was successfully treated with melphalan. Similar to what was observed in the patient, the pMM cells growing

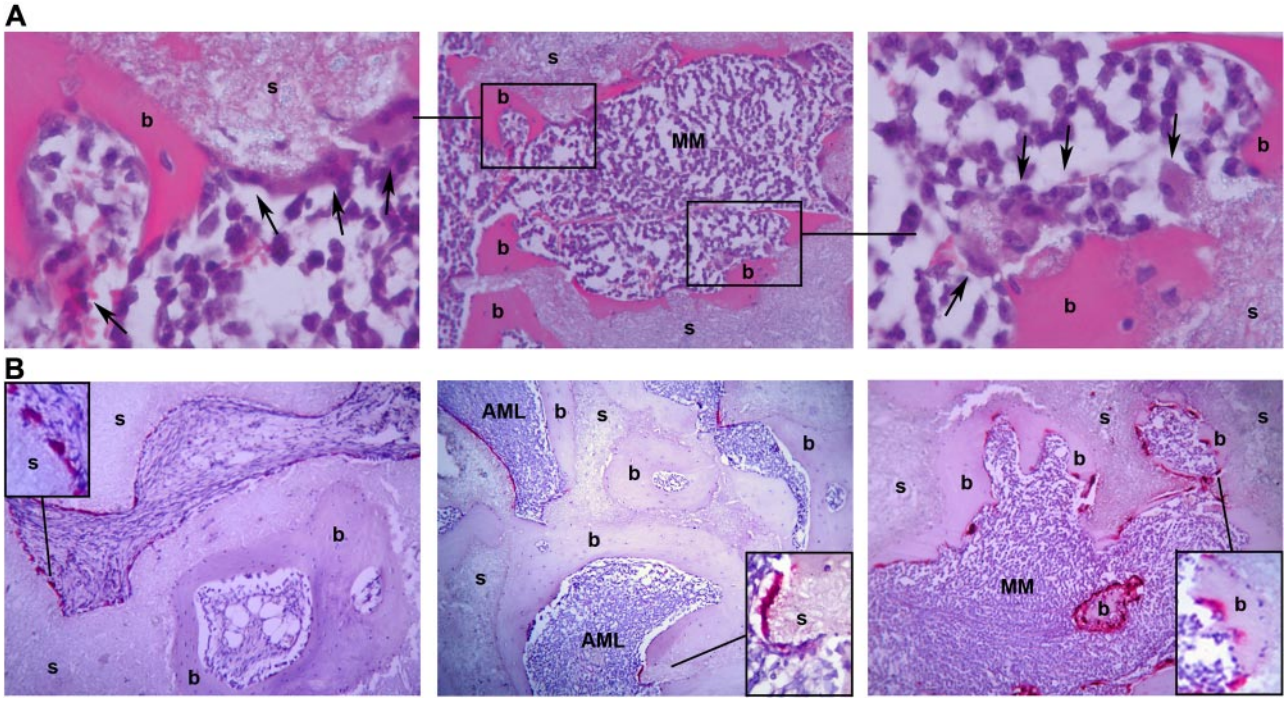

Figure 3. Engraftment of pMM cells in humanized mice coincides with osteolysis. (A) H&E staining shows an irregular bone surface with osteoclast-like cells (arrows). Shown is a representative slide (middle panel) of an MM-infiltrated ossicle (s) covered with bone (b). The left and right panels show the boxed areas at higher magnification. (B) Analysis of control (left panel)–, pAML (middle panel)–, and pMM (right panel)–engrafted ossicles for the presence of osteoclasts by tartrate-resistant acidic phosphatase staining. Shown are representative slides of a control, pMM-, and pAML-engrafted ossicle stained for tartrate-resistant acidic phosphatase.

in the scaffolds showed only minor responses to dexamethasone and bortezomib, but were highly sensitive to melphalan, with virtual elimination of the tumors in 2 of 3 mice (Figure 5A-B). In addition, a strong reduction of tumor mass was observed in a third mouse; however, this mouse relapsed within 4 weeks (Figure 5C). To determine whether the dexamethasone- or bortezomib-unresponsive tumors (Figure 5A-B) could be regressed by novel targeted therapies, the mice were subsequently treated with a novel therapeutic human CD38 mAb, daratumumab.[31] A single injection of daratumumab resulted in complete remission in 3 of 4 mice and a reduction of the tumor load by 50% in 1 of the bortezomib-treated mice (Figure 5D).

We also tested therapeutic intervention on pMM cells from patients 4 and 7 growing in the mouse model representing the 2 ends of the spectrum: that is, patient 4 was a newly diagnosed, untreated MM patient and patient 7 was a plasma cell leukemia relapse patient after melphalan, prednisone, and thalidomide treatment (supplemental Table 1). The pMM-bearing mice of patient 4 responded well to all different treatments, including daratumumab, although they responded best to doxorubicin (Figure 5E). In contrast, in mice bearing MM tumors of patient 7, there was no response to any of the treatments (Figure 5F), including to melphalan and dexamethasone, which were also not effective in the clinical treatment. The aggressive phenotype of the myeloma cells in patient 7 was further reflected in the very high percentage of circulating $CD138^+$ cells (approximately 70% of total blood cells) and the ability to accumulate in the mouse BM in PBS-treated mice, a phenomenon that we did not observe in any of the other MM samples studied. Interestingly, whereas the percentage of $CD138^+$ cells circulating in the blood and BM of the patient 7 MM-bearing mice that received the chemotherapeutic drugs was only slightly reduced, daratumumab treatment resulted in very low percentages of $CD138^+$ cells in the blood and BM (Figure 5G). This mouse model recapitulates the MM phenotype, exhibiting similar characteristics of growth and responses to treatment as observed in MM patients.

Discussion

Over the past 2 decades, many advances have been made in unraveling the components of the hematopoietic niche. However, most of this knowledge is based on transgenic murine models that do not take species-specific ontogeny into account. Although these models have increased our understanding how a specialized microenvironment might regulate HSC and LSC biology, the fact that they do not simulate the human environment impedes translation into clinical applications,[1,2,10,11,14,15,32] suggesting a need for more suitable human models. In the present study, we report the development of a unique and novel mouse model with which to study the human hematopoietic niche in the context of both normal and malignant hematopoiesis.

We observed that the generation of human bone from MSCs in BCP scaffolds, as described previously,[17] creates an environment capable of supporting both murine and human hematopoiesis (Figure 1). We not only observed that $CD34^+$ hematopoietic progenitor cells themselves can engraft, but that hematopoietic cells of distinct lineages are also generated. Consistent with recent murine data,[33] this indicates that the human BM microenvironment engineered in our scaffolds serves as a functional hematopoietic niche and supports the engraftment and growth of hematopoietic (precursor) cells.

A highly important property of our new model is that it also serves as an optimal niche for the engraftment and outgrowth of

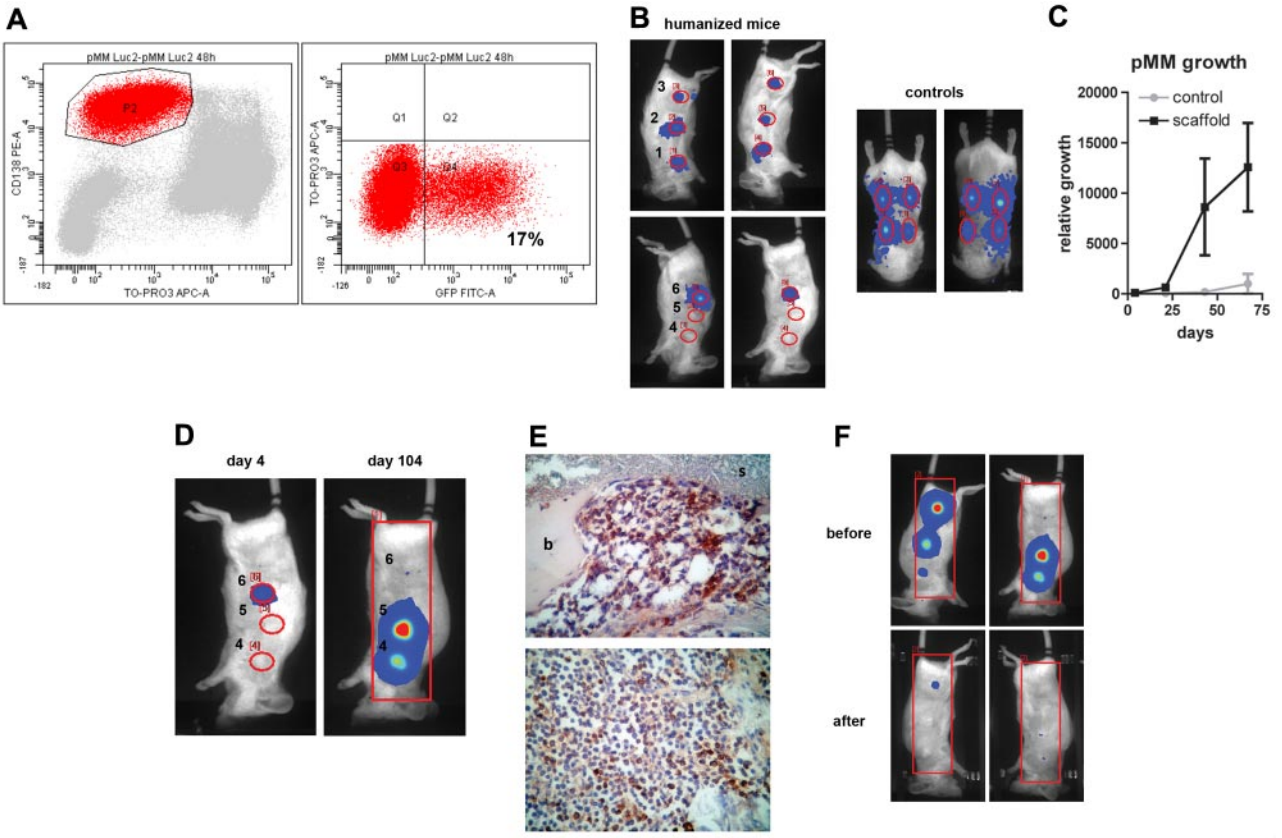

Figure 4. Primary MM cells can be luciferase gene marked, which allows real-time analysis of pMM cell growth. (A) Mononuclear cells of patient 3 were gene marked with luciferase and green fluorescent protein (GFP). Transduction efficiency was analyzed using anti–CD138-PE, TO-PRO-3-iodide, and green fluorescent protein 48 hours after transduction. (B-F) Humanized mice were created by implanting mice with 4 MSC-loaded BCP constructs (sites 2-5) and 2 controls, 1 loaded with MSCs and exposed to 30 Gy of x-rays before implantation (site 1) and the other without MSCs (site 6). Humanized and control mice (ie, mice without ossicles) were inoculated with luciferase-marked pMM cells of patient 3 at 4 sites directly into the ossicle (sites 1-3 and 6) or subcutaneously, respectively, and followed by BLI. (B) BLI images from humanized and control mice 4 days after injection. (C) Tumor growth was determined by average photon emission intensity measured for a region of interest in time. The results are expressed as relative growth with the intensity at day 4 set to 100. The lines represent the mean signal of 2 mice ± SD. (D) BLI images of a representative mouse at day 4 (left panel) and day 104 (right panel) after injection with transduced pMM cells, indicating migration of pMM cells to noninjected sites 4 and 5. (E) Immunohistochemical analysis of ossicles for luciferase with the scaffold material (s) covered with bone (b) and infiltrated by pMM cells. (F) A pMM-carrying humanized mouse was subjected to total body irradiation (6 Gy x-rays) and analyzed by BLI 2 weeks before and after irradiation.

primary MM cells (Figure 2). MM is a malignancy that, despite genetic alterations such as translocations and mutations, remains dependent on the BM microenvironment. The bidirectional interactions of MM cells with the cellular and extracellular components of the BM microenvironment activate a broad range of proliferative and antiapoptotic signaling pathways.[22,23] Whereas xenotransplantation models to study pMM have been developed previously[34-37] and to a certain extent can be used for preclinical evaluation of novel agents, they only offer minimal options with which to investigate the contribution of the BM microenvironment to the pathogenesis of MM. The fact that our present model is based on human MSCs to create a humanized environment provides opportunities for genetic manipulation of the microenvironment by either overexpressing or silencing putative niche-specific genes in MSCs.

Another advantage of our model is the incorporation of BLI as a highly sensitive method for monitoring the tumor load compared with monitoring human heavy or light chains in mouse sera, which is used as an indicator of MM burden in other xenotransplantation models.[34-37] BLI not only allows us to follow engraftment and the dynamics of pMM outgrowth at the original site of inoculation, but also to monitor the secondary spreading of the disease (Figure 4). This provides a more accurate exploration of several novel chemo- and immunotherapy modalities, including targeted immunotherapy with the CD38 Ab daratumumab. Furthermore, the observation that the drug responses of pMM-bearing mice and the corresponding MM patients are remarkably similar (Figure 5) is encouraging in view of potential development of this model into a monitoring system to personalize therapeutic intervention.

This novel and unique human-mouse hybrid model provides unprecedented opportunities to investigate the essential interactions of (tumor) cells with the human BM microenvironment, which will contribute to a better understanding of the influence of the microenvironment on normal and malignant hematopoiesis, and to assess and personalize treatment strategies.

Acknowledgments

The authors thank K. Hesp and G. Geelen for excellent animal care in the central animal facility of the University of Utrecht and Dr P. J. Coffer for critical reading of the manuscript. The RAG2$^{-/-}\gamma_c^{-/-}$ mice were originally obtained from AMCAS BV, Amsterdam, The Netherlands.

This work was supported by grants from Genmab, the Vanderes Foundation, and the Multiple Myeloma Research Foundation (to A.C.M.M.).

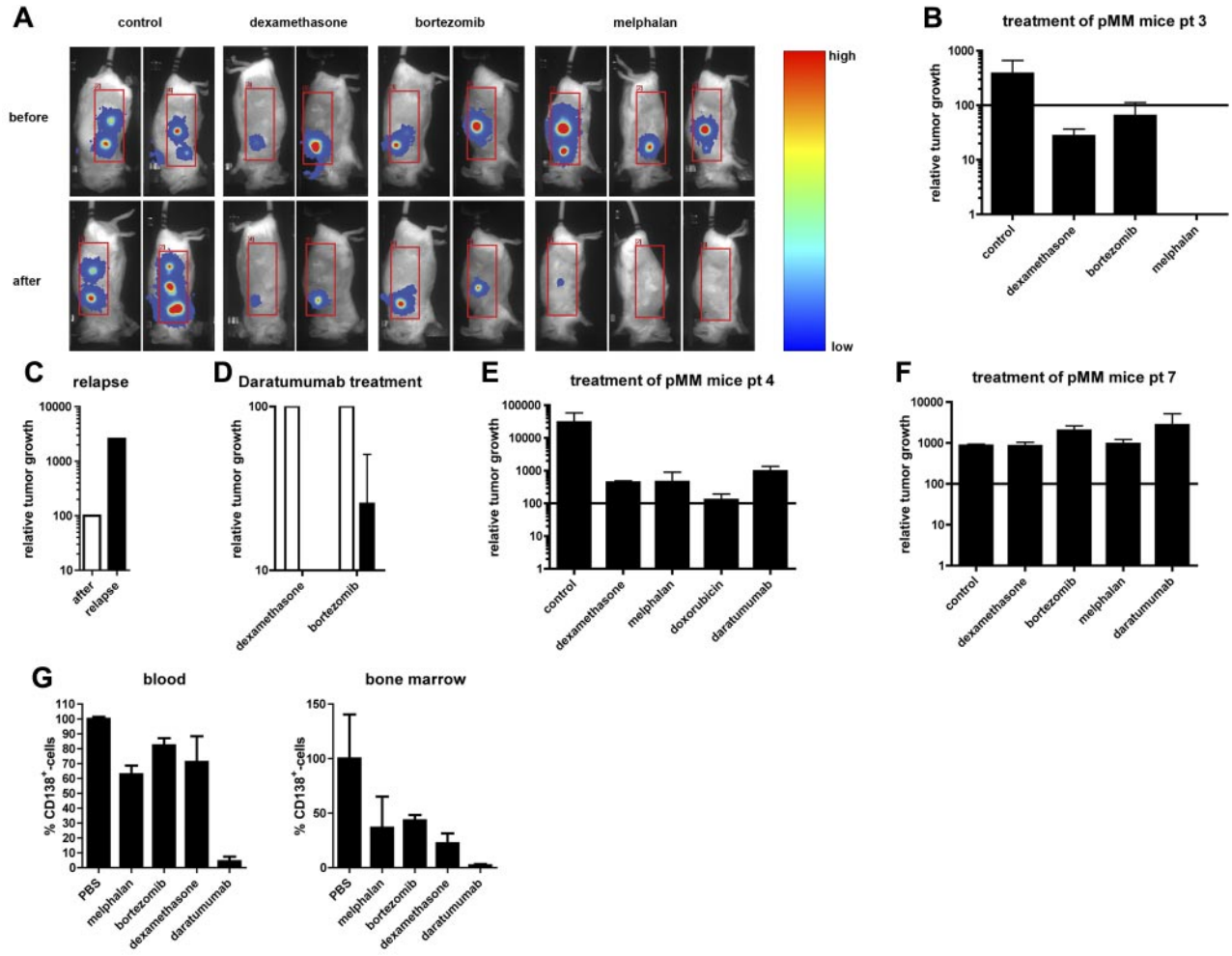

Figure 5. BLI allows visualization of therapy in pMM-bearing mice. (A) Eight weeks after implantation, humanized mice were inoculated with luciferase-marked pMM cells (patient 3) and followed by BLI in time. Seven weeks after tumor inoculation, mice were treated as indicated. Shown are BLI images of representative mice before (week 7; top panels) and 2 weeks after treatment (week 9; bottom panels). (B) Quantification of the therapeutic intervention of mice inoculated with luciferase-marked pMM cells of patient 3. (C) Quantification of the tumor regression (black bar) of a melphalan-treated pMM-bearing mice of patient 3. Results are expressed as relative tumor growth with the growth after treatment (white bar) set to 100. (D) Quantification of daratumumab-treated (black bars) pMM-bearing mice of patient 3, which barely responded to dexamethasone (n = 2) or bortezomib (n = 2). Results are expressed as relative tumor growth with the growth before intervention (white bars) set to 100. (E) Quantification of treatment of mice (n = 2 for control, melphalan, and doxorubicin, and n = 3 for dexamethasone and daratumumab) inoculated with luciferase-marked pMM cells of patient 4. (F) Quantification of treatment of mice (all groups n = 2) inoculated with luciferase-marked pMM cells of patient 7. (G) Analysis of blood (left) and BM (right) for human CD138$^+$ cells after euthanasia of the patient 7 pMM-bearing mice. Results are expressed as the percentage of CD138$^+$ cells with the percentage in the PBS-treated group set to 100. In panels B, E, and F, results are expressed as relative tumor growth with the growth before intervention set to 100 (solid line). In panels B and D through G, bars represent the means ± SEM of the mice within a therapeutic group after treatment.

Authorship

Contribution: R.W.J.G. performed the research, analyzed the data, and wrote the manuscript; W.A.N. performed the research and analyzed the data; R.A.R. provided patient information and wrote the manuscript; H.-J.P., L.A., F.M.H., P.M., B.v.K., and H.R. performed the research; J.F.v.V., A.C.B., E.v.B., and A.B. analyzed the clinical and mouse data; H.Y. and J.D.d.B. provided the scaffold material and technical assistance; M.d.W. and P.W.H.I.P. provided the daratumumab and designed the experiments; J.J.S. and H.M.L. provided the patient material and clinical information; and T.M. and A.C.M.M. designed and supervised the research and wrote the manuscript.

Conflict-of-interest disclosure: H.Y. is an employee and shareholder of Xpand Biotechnology BV. J.D.d.B. is a founder of Xpand Biotechnology BV and a member of its scientific advisory board. M.d.W. and P.W.H.I.P. are Genmab employees and own Genmab warrants and/or stock. The remaining authors declare no competing financial interests.

Correspondence: Anton C. M. Martens, PhD, Department of Cell Biology, University Medical Center Utrecht, Heidelberglaan 100, 3584 CX, Utrecht, The Netherlands; e-mail: a.martens@umcutrecht.nl.

References

1. Yin T, Li L. The stem cell niches in bone. *J Clin Invest.* 2006;116(5):1195-1201.
2. Kiel MJ, Morrison SJ. Uncertainty in the niches that maintain haematopoietic stem cells. *Nat Rev Immunol.* 2008;8(4):290-301.
3. Oh IH, Kwon KR. Concise review: multiple niches for hematopoietic stem cell regulations. *Stem cells.* 2010;28(7):1243-1249.
4. Bianco P. Bone and the hematopoietic niche: a

tale of two stem cells. *Blood.* 2011;117(20):5281-5288.

5. Hanahan D, Weinberg RA. Hallmarks of cancer: the next generation. *Cell.* 2011;144(5):646-674.
6. Pietras K, Ostman A. Hallmarks of cancer: interactions with the tumor stroma. *Exp Cell Res.* 2010;316(8):1324-1331.
7. Roberts KG, Mullighan CG. How new advances in genetic analysis are influencing the understanding and treatment of childhood acute leukemia. *Curr Opin Pediatr.* 2011;23(1):34-40.
8. Downing JR, Shannon KM. Acute leukemia: a pediatric perspective. *Cancer Cell.* 2002;2(6):437-445.
9. Röllig C, Bornhauser M, Thiede C, et al. Long-term prognosis of acute myeloid leukemia according to the new genetic risk classification of the European LeukemiaNet recommendations: evaluation of the proposed reporting system. *J Clin Oncol.* 2011;29(20):2758-2765.
10. Shiozawa Y, Havens AM, Pienta KJ, Taichman RS. The bone marrow niche: habitat to hematopoietic and mesenchymal stem cells, and unwitting host to molecular parasites. *Leukemia.* 2008;22(5):941-950.
11. Lane SW, Scadden DT, Gilliland DG. The leukemic stem cell niche: current concepts and therapeutic opportunities. *Blood.* 2009;114(6):1150-1157.
12. Konopleva MY, Jordan CT. Leukemia stem cells and microenvironment: biology and therapeutic targeting. *J Clin Oncol.* 2011;29(5):591-599.
13. Zipori D. The hemopoietic stem cell niche versus the microenvironment of the multiple myeloma-tumor initiating cell. *Cancer Microenviron.* 2010;3(1):15-28.
14. Carlesso N, Cardoso AA. Stem cell regulatory niches and their role in normal and malignant hematopoiesis. *Curr Opin Hematol.* 2010;17(4):281-286.
15. Lévesque JP, Helwani FM, Winkler IG. The endosteal 'osteoblastic' niche and its role in hematopoietic stem cell homing and mobilization. *Leukemia.* 2010;24(12):1979-1992.
16. Peerani R, Zandstra PW. Enabling stem cell therapies through synthetic stem cell-niche engineering. *J Clin Invest.* 2010;120(1):60-70.
17. Prins HJ, Rozemuller H, Vonk-Griffioen S, et al. Bone-forming capacity of mesenchymal stromal cells when cultured in the presence of human platelet lysate as substitute for fetal bovine serum. *Tissue Eng Part A.* 2009;15(12):3741-3751.
18. Geuze RE, Prins HJ, Oner FC, et al. Luciferase labeling for multipotent stromal cell tracking in spinal fusion versus ectopic bone tissue engineering in mice and rats. *Tissue Eng Part A.* 2010;16(11):3343-3351.
19. Reijmers RM, Groen RW, Rozemuller H, et al. Targeting EXT1 reveals a crucial role for heparan sulfate in the growth of multiple myeloma. *Blood.* 2010;115(3):601-604.
20. Chesi M, Robbiani DF, Sebag M, et al. AID-dependent activation of a MYC transgene induces multiple myeloma in a conditional mouse model of post-germinal center malignancies. *Cancer Cell.* 2008;13(2):167-180.
21. Mitsiades CS, Mitsiades NS, Munshi NC, Richardson PG, Anderson KC. The role of the bone microenvironment in the pathophysiology and therapeutic management of multiple myeloma: interplay of growth factors, their receptors and stromal interactions. *Eur J Cancer.* 2006;42(11):1564-1573.
22. Hideshima T, Mitsiades C, Tonon G, Richardson PG, Anderson KC. Understanding multiple myeloma pathogenesis in the bone marrow to identify new therapeutic targets. *Nat Rev Cancer.* 2007;7(8):585-598.
23. Podar K, Chauhan D, Anderson KC. Bone marrow microenvironment and the identification of new targets for myeloma therapy. *Leukemia.* 2009;23(1):10-24.
24. Ganem NJ, Pellman D. Limiting the proliferation of polyploid cells. *Cell.* 2007;131(3):437-440.
25. Aylon Y, Oren M. p53: Guardian of ploidy. *Mol Oncol.* 2011;5(4):315-323.
26. Giuliani N, Rizzoli V, Roodman GD. Multiple myeloma bone disease: Pathophysiology of osteoblast inhibition. *Blood.* 2006;108(13):3992-3996.
27. Edwards CM, Zhuang J, Mundy GR. The pathogenesis of the bone disease of multiple myeloma. *Bone.* 2008;42(6):1007-1013.
28. Roodman GD. Pathogenesis of myeloma bone disease. *J Cell Biochem.* 2010;109(2):283-291.
29. Yaccoby S. Osteoblastogenesis and tumor growth in myeloma. *Leuk Lymphoma.* 2010;51(2):213-220.
30. Rozemuller H, van der Spek E, Bogers-Boer LH, et al. A bioluminescence imaging based in vivo model for preclinical testing of novel cellular immunotherapy strategies to improve the graft-versus-myeloma effect. *Haematologica.* 2008;93(7):1049-1057.
31. de Weers M, Tai YT, van der Veer MS, et al. Daratumumab, a novel therapeutic human CD38 monoclonal antibody, induces killing of multiple myeloma and other hematological tumors. *J Immunol.* 2011;186(3):1840-1848.
32. Raaijmakers MH. Niche contributions to oncogenesis: emerging concepts and implications for the hematopoietic system. *Haematologica.* 2011;96(7):1041-1048.
33. Fujita A, Migita M, Ueda T, Ogawa R, Fukunaga Y, Shimada T. Hematopoiesis in regenerated bone marrow within hydroxyapatite scaffold. *Pediatr Res.* 2010;68(1):35-40.
34. Urashima M, Chen BP, Chen S, et al. The development of a model for the homing of multiple myeloma cells to human bone marrow. *Blood.* 1997;90(2):754-765.
35. Yaccoby S, Barlogie B, Epstein J. Primary myeloma cells growing in SCID-hu mice: a model for studying the biology and treatment of myeloma and its manifestations. *Blood.* 1998;92(8):2908-2913.
36. Yata K, Yaccoby S. The SCID-rab model: a novel in vivo system for primary human myeloma demonstrating growth of CD138-expressing malignant cells. *Leukemia.* 2004;18(11):1891-1897.
37. Calimeri T, Battista E, Conforti F, et al. A unique three-dimensional SCID-polymeric scaffold (SCID-synth-hu) model for in vivo expansion of human primary multiple myeloma cells. *Leukemia.* 2011;25(4):707-711.